Bimetallic Fe–Ir and Trimetallic Fe–Ir–Au Carbonyl Clusters Containing Hydride and/or Phosphine Ligands: Syntheses, Structures and DFT Studies

Bimetallic Fe-Ir and Trimetallic Fe-Ir-Au Carbonyl Clusters Containing Hydride and/or Phosphine Ligands: Syntheses, Structures and DFT Studies

Beatrice Berti,[1] Marco Bortoluzzi,[2] Cristiana Cesari,[1] Cristina Femoni,[1] Mohammad Hayatifar,[1] Maria Carmela Iapalucci,[1] Stefano Zacchini[1]*

[1] Dipartimento di Chimica Industriale "Toso Montanari", Università di Bologna, Viale Risorgimento 4 - 40136 Bologna, Italy. E-mail: stefano.zacchini@unibo.it

[2] Dipartimento di Scienze Molecolari e Nanosistemi, Ca' Foscari University of Venice, Dorsoduro 2137, 30123, Venezia, Italy

ABSTRACT: The reaction of $[HFe_4(CO)_{12}(IrCOD)]^{2-}$ (**1**) with CO at ambient conditions afforded $[HFe_4Ir(CO)_{14}]^{2-}$ (**2**), that, in turn, reacted with $HBF_4{\cdot}Et_2O$ affording $[Fe_4Ir(CO)_{15}]^{-}$ (**3**). **1** reacted with a slight excess of PPh_3 resulting in a mixture of $[HFe_2Ir_2(CO)_{10}(PPh_3)_2]^{-}$ (*ca.* 37%) (**5**) and $[H_2Fe_3Ir(CO)_{10}(PPh_3)_2]^{-}$ (*ca.* 63%) (**6**). **5** and **6** co-crystallized as their $[NEt_4][H_{1+x}Fe_{2+x}Ir_{2-x}(CO)_{10}(PPh_3)_2]{\cdot}CH_2Cl_2$ (x = 0.63) salt. The reaction of **1** with $Au(PPh_3)Cl$ afforded $[Fe_3Ir(CO)_{12}(AuPPh_3)]^{2-}$ (**7**). The related hydride $[HFe_3Ir(CO)_{12}]^{2-}$ (**9**) was prepared from the reaction of $[HFe_4(CO)_{12}]^{3-}$ (**8**) with $[Ir(COE)_2Cl]_2$ (COE = cyclo-octene). For sake of comparison, $[HFe_3Co(CO)_{12}]^{2-}$ (**10**) was obtained from **8** and $Co_2(CO)_8$. All the new clusters have been fully characterized *via* IR, ^1H,$^{13}C\{^1H\}$ and $^{31}P\{^1H\}$ NMR spectroscopies and their structures determined by means of single crystal X-ray crystallography. Possible isomers have been investigated by DFT calculations.

Keywords: Heterometallic cluster; Carbonyl; Iron; Iridium; Hydride

Introduction

Several bimetallic Fe-Ir carbonyl clusters are known, including both homoleptic and heteroleptic species [1-12]. In addition, a few trimetallic Fe-Ir-Au carbonyl clusters have been also reported [5,11,13,14]. The introduction of AuL fragments into metal carbonyl clusters was widely investigated in view of their isolobal analogy with the hydride ligand and because of aurophilic interactions [15-33].

Organometallic clusters containing different metals and ligands are interesting for the activation and transformation of small organic species as well as for the anchoring on supports [34-37]. Moreover, bimetallic clusters have been employed as precursors for supported bimetallic catalysts, leading to an accurate control of the sizes and compositions of the resulting metal nanoparticles [38-50]. In particular, Fe-Ir nanostructured catalytic materials derived from bimetallic carbonyl clusters have been employed for the preparation of methanol from synthesis gas [51-53], the water-gas shift reaction [54] and ethylene hydroformyltaion [55].

We recently reported the synthesis and molecular structure of the pentanuclear $[HFe_4(CO)_{12}(IrCOD)]^{2-}$ (**1**) bimetallic hydride carbonyl cluster, as well as its reactions with strong acids [1]. These resulted, first, in the isonuclear dihydride $[H_2Fe_4(CO)_{12}(IrCOD)]^{-}$ and, then, the tetranuclear dihydride $[H_2Fe_3(CO)_{10}(IrCOD)]^{-}$ was obtained via formal oxidative elimination of a $Fe(CO)_2$ fragment. Herein, we report the study of the reactions of **1** with CO, PPh_3 and $Au(PPh_3)Cl$ which result in new bimetallic and trimetallic clusters. Their structures have been determined by means of Single-Crystal X-ray Diffraction (SC-XRD). Possible isomers of selected compound here described have been investigated by DFT calculations.

Results and Discussion

The reaction of $[HFe_4(CO)_{12}(IrCOD)]^{2-}$ (**1**) with CO at ambient conditions afforded $[HFe_4Ir(CO)_{14}]^{2-}$ (**2**) via the substitution of the COD ligand with two carbonyls (Scheme 1). Since CO is a stronger π-acid than COD, the ν_{CO} bands of **2** (2030(w), 1970(vs), 1955(sh), 1915(m), 1773(m) cm^{-1} in CH_2Cl_2) moved to considerably higher wavenumbers compared to **1** (1983(m), 1922(vs), 1775(br) cm^{-1} in CH_2Cl_2). The molecular structure of **2** was ascertained by means of SC-XRD (Figure 1 and Table 1).

2 may be described as a Fe_4Ir trigonal bipyramid (TBP), where the unique Ir atom occupies an equatorial position. It is noteworthy that the parent cluster **1** adopted a TBP structure, but the Ir atom was located on an apical position [1]. From a simple thermodynamic point of view, Ir-Fe bonds should be stronger than Fe-Fe ones. Thus, the location of Ir in an equatorial position of **2** should be favored respect to the apical isomer. Indeed, the equatorial isomer possesses four Ir-Fe and five Fe-Fe bonds, whereas a purported apical isomer would present three Ir-Fe and six Fe-Fe bonds. Conversely, the apical isomer was found in the case of **1**, because of the presence of the

bulky COD ligand bonded to Ir. For comparison, $[FeIr_4(CO)_{15}]^{2-}$, $[FeIr_4(CO)_{13}]^{2-}$ and $[Fe_2Ir_3(CO)_{14}]^-$ displayed TBP structures with the Fe atoms in apical positions [2,7].

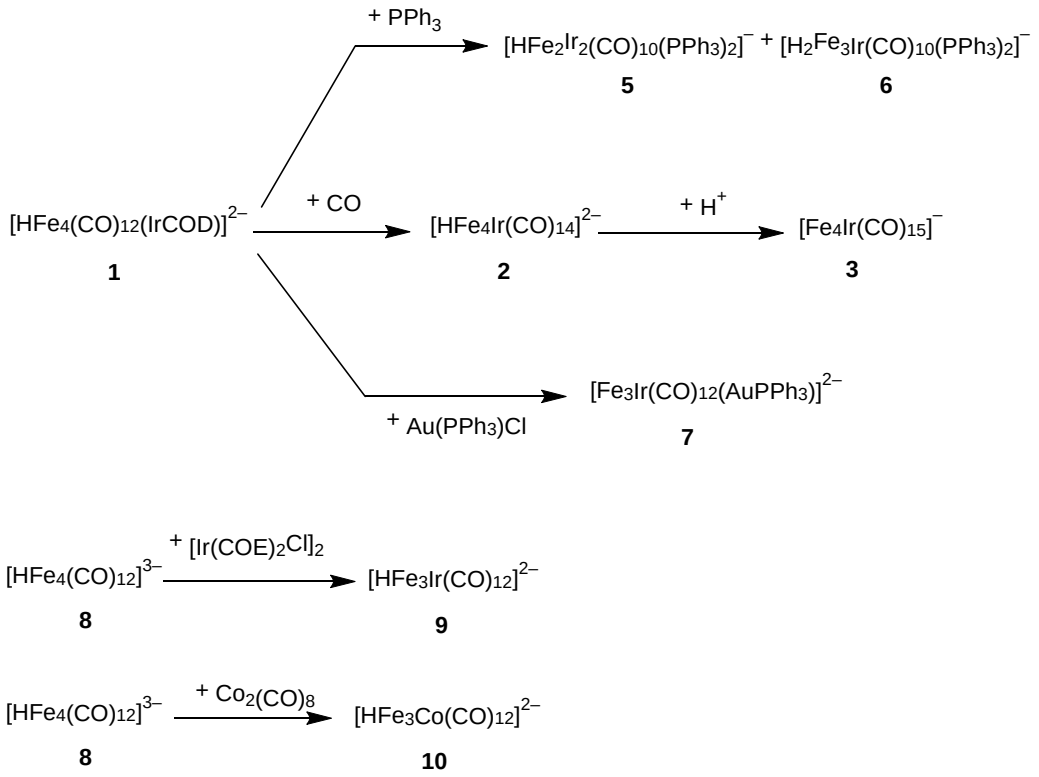

Scheme 1 Synthesis of the cluster described in the paper.

The hydride ligand was located in the Fourier Difference Map and included in the final refinement of the structure. The unique hydride is face-capping on a Fe_3-triangle. The Fe-H distances [1.67(9) Å] are in keeping with those reported in the literature [56]. A similar coordination of the hydride ligand to a Fe_3-face was also found in the TBP cluster $[HFe_5(CO)_{14}]^{3-}$, whose Fe-H distances were in the range 1.70-1.80 Å [51].

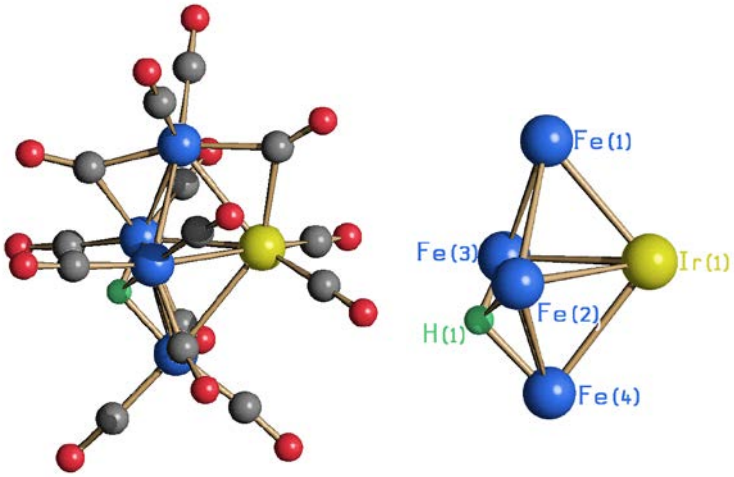

(a) (b)

Fig. 1 (a) Molecular structure of $[HFe_4Ir(CO)_{14}]^{2-}$ (**2**) and (b) its metal core with labeling (blue, Fe; yellow, Ir; grey, C; red, O; green, H).

Table 1 Main bond distances (Å) of **1-10**.

	Fe-Fe	**Fe-M ***	**Fe-H**	**M-H**
$[HFe_4(CO)_{12}(IrCOD)]^{2-}$ (**1**)**	2.5686(13)-2.6376(16) Average 2.153(3)	2.6447(8)-2.73334(11) Average 2.6743(16)	1.79(6)	1.72(9)
$[HFe_4Ir(CO)_{14}]^{2-}$ (**2**)	2.484(5)-2.719(5) Average 2.587(11)	2.617(4)-2.698(4) Average 2.651(8)	1.67(9)	-
$[Fe_4Ir(CO)_{15}]^{-}$ (**3**)	2.611(4)-2.636(4) Average 2.625(9)	2.611(4)-2.780(3) Average 2.658(8)	-	-
$[H_2Fe_4(CO)_{12}(IrCOD)]^{-}$ (**4**)**	2.5514(11)-2.7155(14) Average 2.602(3)	2.6624(7)-2.8207(11) Average 2.7235(17)	1.663(19), 1.669(19), 1.701(19)	1.796(19), 1.904(19)
$[H_2Fe_3(CO)_{10}(IrCOD)]^{-}$**	2.5809(8)-2.6200(7) Average 2.6042(14)	2.6724(5)-2.7940(6) Average 2.7308(10)	1.62(4), 1.76(3), 1.77(3)	1.67(4), 1.76(4)

$[HFe_2Ir_2(CO)_{10}(PPh_3)_2]^-$ (**5**)	2.611(2)	2.573(10)-2.6805(17) Average 2.624(3)	1.696(10)	1.67(4), 1.928(10)
$[H_2Fe_3Ir(CO)_{10}(PPh_3)_2]^-$ (**6**)	2.611(2)-2.738(19) Average 2.69(3)	2.63(2)-2.6805(17) Average 2.65(3)	1.604(9), 1.690(10), 1.696(10)	1.928(10)
$[Fe_3Ir(CO)_{12}(AuPPh_3)]^{2-}$ (**7**)	2.587(5)-2.679(4) Average 2.624(12)	2.602(4)-2.737(5) Average 2.343(14)	-	-
$[HFe_3Ir(CO)_{12}]^{2-}$ (**9**)	2.601(2)-2.626(2) Average 2.617(3)	2.6300(18)-2.7618(18) Average 2.342(3)	1.67(2)	1.81(2)
$[HFe_3Co(CO)_{12}]^{2-}$ (**10**)	2.5352(12)-2.6645(9) Average 2.6214(17)	2.5019(9)-2.5564(11) Average 2.5201(17)	1.66(3)	1.68(5)

* M = Ir (**1-6, 9**), Ir and Au (**7**), Co (**10**).

** From ref. [1].

2 contains 14 CO ligands, 10 terminal and four edge bridging, that is the same stereochemistry of the CO ligands found in $[Fe_2Ir_3(CO)_{14}]^-$ [2]. Conversely, $[HFe_5(CO)_{14}]^{3-}$ displays a slight different geometry of the carbonyls, with 10 terminal, 3 edge bridging and one face-capping [57]. It is likely that the smaller size of Fe compared to Ir and the greater negative charge of $[HFe_5(CO)_{14}]^{3-}$ compared to **2**, that correspond to a higher electron density on the metal centers, favor the rearrangement of a CO ligand from edge-bridging to face-capping.

2 possesses 72 Cluster Valence Electrons (CVE) in agreement with the Effective Atomic Number rule (EAN) for a TBP [58-61]. The same electron count has been found in other TBP Fe-Ir clusters, such as **1**, $[Fe_2Ir_3(CO)_{14}]^-$ and $[FeIr_4(CO)_{13}]^{2-}$ [2,7], as well as homometallic Fe and Ir species, such as $[HFe_5(CO)_{14}]^{3-}$ [57], $Ir_5(CO)_{12}(PPh_3)(Ph)$ [62], $[HIr_5(CO)_{12}]^{2-}$ [63], $Ir_5(CO)_{11}(COD)(Ph)$ and $Ir_5(CO)_9(COD)_2(Ph)$ [64]. Conversely, $[FeIr_4(CO)_{15}]^{2-}$ displays 76 CVE [2], as found in some other TBP carbonyl clusters [65], such as $[Ni_5(CO)_{12}]^{2-}$ [66] and $[Rh_5(CO)_{15}]^-$ [67]. The variable electron count (72 *vs.* 76 CVE) in TBP clusters was previously discussed in the

literature [60]. As a general consideration, 72 CVE is the most typical electron count for TBP clusters in the absence of bulky ligands or electron rich metals. Indeed, 76 CVE are found in the presence of d^{10} or d^9 carbonyl clusters such as $[Ni_5(CO)_{12}]^{2-}$ [66] and $[Rh_5(CO)_{15}]^-$[67]. The $FeIr_4$ core found in $[FeIr_4(CO)_{13}]^{2-}$ and $[FeIr_4(CO)_{15}]^{2-}$ [2,7] is somehow a borderline case. It contains one d^8 and four d^9 metals and, as a consequence, it may form both a 72 CVE as well as a 76 CVE species.

The hydride nature of **2** was further corroborated through ^{1}H NMR spectroscopy, that displayed the presence of a singlet at δ -21.26 ppm at 298 K. This resonance is not affected by the temperature (at least down to 213 K). For comparison, the parent mono-hydride **1** displayed at room temperature a singlet at δ -17.72ppm [1], whereas the unique hydride of $[HFe_5(CO)_{14}]^{3-}$ resonated at δ -18.10 ppm [57].

The hydride location was also confirmed by means of geometry optimizations carried out at DFT level, starting from the experimental X-Ray structure (see **2-eq1** in Figure S1 in Supporting Information). On considering the Fe_4Ir TBP with the Ir atom occupying an equatorial position, isomers with the hydride face-capping on a Fe_2Ir-triangle (**2-eq2** in Figure S1) or located on a Fe-Ir edge (**2-eq3** in Figure S1) were considered, but they resulted less stable than **2-eq1** by about 9.2 and 11.8 kcal mol^{-1}, respectively. DFT calculations also allowed to verify the greater thermodynamic stability of the equatorial position of the Ir fragment. All the isomers of **2** with apical Ir (see **2-ap1**, **2-ap2** and **2-ap3** in Figure S2) resulted less stable than **2-eq1** by 12.5 – 19.0 kcal mol^{-1}. It is worth noting that also for these isomers the most stable hydride location is face-capping on a Fe_3-triangle.

The higher stability of equatorial Ir in compound **2** prompted us to computationally investigate also possible isomers of the previously reported $[HFe_4(CO)_{12}(IrCOD)]^{2-}$ (**1**) cluster, where apical Ir was experimentally observed. DFT calculations allowed to optimize the geometry of a second isomer with equatorial Ir (**1-eq**), that resulted slightly more stable by about 2.6 kcal mol^{-1} with respect to the DFT-optimized geometry of the apical isomer (**1-ap**). It can be therefore tentatively supposed that the experimentally isolated compound **1** is a kinetic product. Calculations do not however give any information about the kinetic barrier related to the possible isomerization, therefore we cannot predict if such a process could occur. The experimental evidences do not indicate the presence of **1-eq** in the reaction mixture.

As observable in Figure S3, the preferred position for the hydride is face-capping on a Fe_2Ir-triangle in both the isomers, differently from compound **2**. These outcomes suggest that the formal

replacement of COD with two carbonyl ligands reduces the tendency of Ir with respect to Fe to participate to the formation of M-H bonds.

2 reacted with strong acids such as $HBF_4 \cdot Et_2O$ affording the pentanuclear mono-anion $[Fe_4Ir(CO)_{15}]^-$ (**3**). **3** retains the TBP 72 CVE structure of **2** with the unique Ir atom in the equatorial plane (Figure 2 and Table 1). Among the 15 CO ligands, three are edge bridging on the $IrFe_2$ equatorial plane, and twelve are in terminal positions. In this respect, **3** may be regarded as composed by a $[Fe_2Ir(\mu\text{-}CO)_3(CO)_6]^-$ core capped by two $Fe(CO)_3$ fragments. Conversely, the TBP 76 CVE cluster $[FeIr_4(CO)_{15}]^{2-}$ displayed nine terminal and six edge bridging carbonyls [2], as also observed in other isoelectronic and isostructural species such as $[RuIr_4(CO)_{15}]^{2-}$ [68] and $[RuRh_4(CO)_{15}]^{2-}$ [69]. It is likely that the presence of four additional electron in these 76 CVE TBP clusters favors back-donation from the metal core and, thus, bridging CO ligands, compared to 72 CVE species such as **3**.

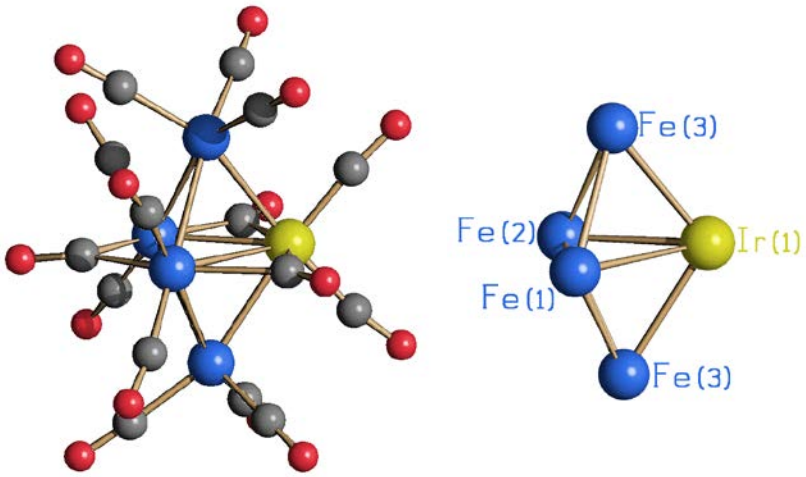

(a) (b)

Fig. 2 (a) Molecular structure of $[Fe_4Ir(CO)_{15}]^-$ (**3**) and (b) its metal core with labeling (blue, Fe; yellow, Ir; grey, C; red, O).

It is noteworthy that **1** under the same conditions was protonated to the di-hydride $[H_2Fe_4(CO)_{12}(IrCOD)]^-$ (**4**) and subsequently, by increasing the amount of acid employed, transformed into $[H_2Fe_3(CO)_{10}(IrCOD)]^-$, via formal oxidative elimination of $Fe(CO)_2$ [1]. DFT calculations confirmed that the replacement of COD with two carbonyls makes the dianionic cluster less basic, therefore the protonation is less favorable: ΔG(**2-eq1** + $H^+ \rightarrow$ **2-prot1**) - ΔG(**1-ap** + $H^+ \rightarrow$ **4**) = 5.9 kcal mol^{-1}. The DFT-optimized structures of **2-prot** obtained starting from the most

stable isomer of **2** are shown in Figure S4. As observable, calculations confirmed the scarce tendency of the $[Ir(CO)_2]$ fragment in the cluster to form Ir-H bonds. Such a behavior is probably related to the lower electron density on the metal centre achieved by replacing COD with two CO. The computed Hirshfeld charge on Ir for $[Ir(COD)]^+$ is 0.389 a.u., while for $[Ir(CO)_2]^+$ is 0.479 a.u.

The reaction of **1** with PPh_3 proceeded very slowly and with lower yields, compared to the reaction with CO which was fast and almost quantitative. Indeed, **1** reacted only with a slight excess of PPh_3 after several days at room temperature, affording mainly non-soluble decomposition products. Eventually, after work-up of the reaction mixture, it was possible to isolate in low yields (ca. 26% based on Fe) a mixture of $[HFe_2Ir_2(CO)_{10}(PPh_3)_2]^-$ (*ca.* 37%) (**5**) and $[H_2Fe_3Ir(CO)_{10}(PPh_3)_2]^-$ (*ca.* 63%) (**6**). **5** and **6** co-crystallized as their $[NEt_4][H_{1+x}Fe_{2+x}Ir_{2-x}(CO)_{10}(PPh_3)_2]\cdot CH_2Cl_2$ (x = 0.63) salt and, therefore, their structures were determined by SC-XRD (Figure 3 and Table 1).

Both clusters displayed a tetrahedral metal core composed of a $M_3(\mu_3\text{-H})(\mu\text{-CO})_3(CO)_4(PPh_3)_2$ basal unit (M_3 = $FeIr_2$ in **5**, Fe_2Ir in **6**) connected to a $Fe(CO)_3$ apical moiety. The two PPh_3 ligands of **5** were bonded to the two Ir atoms in the basal plane. Formally, **6** was obtained by replacing one of these Ir atoms with a FeH unit. The additional hydride of **6** was μ_3-coordinated to the unique Fe_3 triangular face. **5** and **6** were isoelectronic possessing 60 CVE as expected for a tetrahedron [59].

The only tetrahedral Fe_2Ir_2 cluster previously reported was the dianion $[Fe_2Ir_2(CO)_{12}]^{2-}$ [5], that was composed by a $FeIr_2(\mu\text{-CO})_3(CO)_6$ basal unit connected to a $Fe(CO)_3$ apical moiety. Formally, **5** arises from $[Fe_2Ir_2(CO)_{12}]^{2-}$ by substitution of two terminal carbonyls on the basal unit with two PPh_3 ligands and addition of a μ_3-H hydride to the same unit. Indeed, based on the isolobal analogy, a $[AuPPh_3]^+$ fragment was added on the same $FeIr_2$ face of $[Fe_2Ir_2(CO)_{12}]^{2-}$ affording $[Fe_2Ir_2(CO)_{12}(AuPPh_3)]^-$ [5].

The structure of **6** can be compared to $[H_2Fe_3Ir(CO)_{10}(COD)]^-$ [1], that consists of a $Fe_2Ir(\mu\text{-CO})_3(CO)_4(COD)$ basal unit connected to a $Fe(CO)_3$ apical moiety. In this respect, the major difference from **6** is the presence of a chelating COD ligand on Ir instead of two terminal PPh_3 ligands (one on Ir, one on a basal Fe) as found in **6**. Moreover, $[H_2Fe_3Ir(CO)_{10}(COD)]^-$ displays one μ_3-H on the Fe_2Ir basal unit (as in **6**), whereas the second hydride is μ-H connected to the $Ir\text{-}Fe_{apical}$ edge, and not μ_3-H bonded to the $(Fe_{basal})_2(Fe_{apical})$ face as in **6**. This slight difference in the stereochemistry of the two hydride ligands in **6** and $[H_2Fe_3Ir(CO)_{10}(COD)]^-$ may be ascribed to the

formal replacement of two terminal phosphines with a chelating COD ligand. Nonetheless, it must be remarked that often hydrides in such clusters are fluxional and, sometimes, different isomers may also exist.

Both ^{1}H and $^{31}P\{^{1}H\}$ NMR spectra of the $[NEt_4][H_{1+x}Fe_{2+x}Ir_{2-x}(CO)_{10}(PPh_3)_2]\cdot CH_2Cl_2$ (x =0.63) crystals dissolved in CD_3COCD_3 displayed two distinct resonances at all temperatures, one attributable to **5** and the other to **6**, suggesting, at least for **6**, a rapid exchange in solution that makes equivalent the two PPh_3 and hydride ligands.

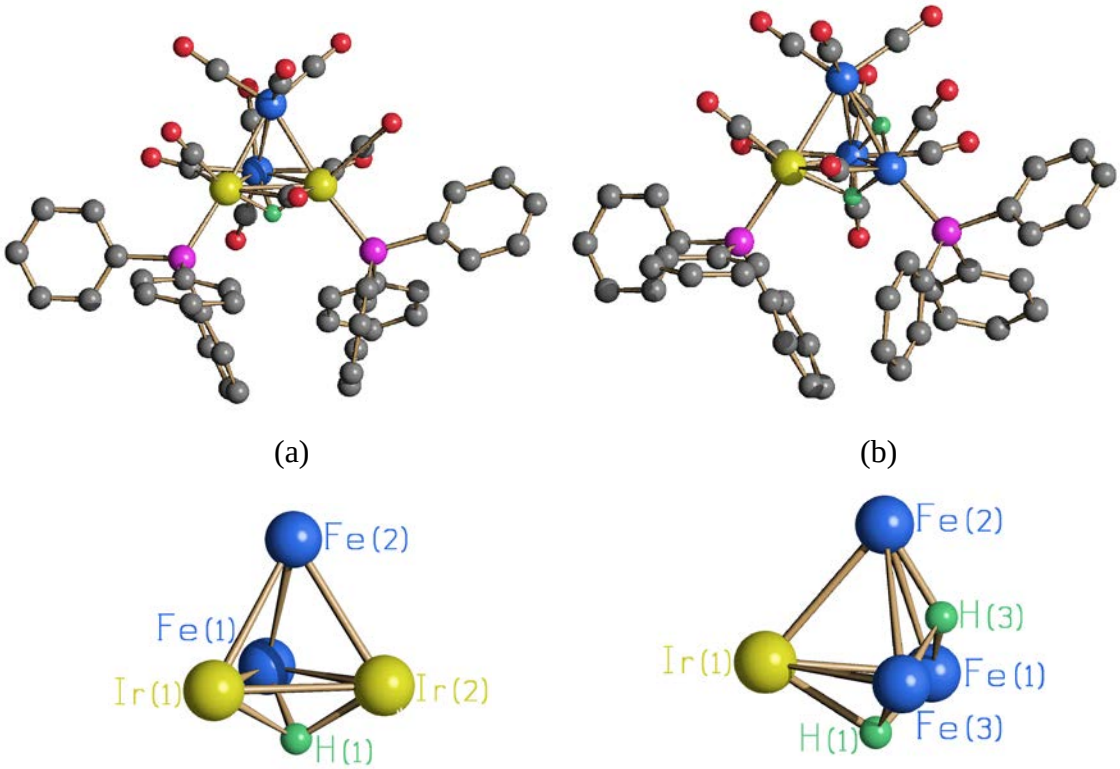

Fig. 3 Molecular structures of (a) $[HFe_2Ir_2(CO)_{10}(PPh_3)_2]^-$ (**5**) and (b) $[H_2Fe_3Ir(CO)_{10}(PPh_3)_2]^-$ (**6**), and their metal-hydride cages with labeling (blue, Fe; yellow, Ir; grey, C; red, O; green, H; purple, P). H-atoms bonded to Ph-rings have been omitted for clarity.

DFT calculations helped to locate the hydride ligands in the clusters **5** and **6**. The DFT-optimized structures are shown in Figure S5. The μ_3-H ligands on $FeIr_2$ and Fe_2Ir faces were obtained for **5** and **6**, respectively. It is worth noting that the coordination of a good σ-donor such as PPh_3 to Ir allows it to participate to M-H bonds, in agreement with previous considerations. The optimized position of the second hydride in **6** is on a Fe-Fe edge, whereas SC-XRD suggested its location on a Fe_3 face. It must be remarked that location of hydrides by SC-XRD in the presence of

heavy atoms and disorder is not an easy task. This may explain the slight discrepancy between SC-XRD and DFT for the second hydride of **6**, that is only partially present in the disorder model of $[NEt_4][H_{1+x}Fe_{2+x}Ir_{2-x}(CO)_{10}(PPh_3)_2]\cdot CH_2Cl_2$ (x = 0.63).

The reaction of **1** with $Au(PPh_3)Cl$ afforded $[Fe_3Ir(CO)_{12}(AuPPh_3)]^{2-}$ (**7**). Its molecular structure was determined by SC-XRD (Figure 4 and Table 1). **7** possessed a TBP structure, with Ir in the equatorial plane and Au in an apical position. Alternatively, it could be described as the result of the addition of a $[AuPPh_3]^+$ fragment to a tetrahedral $[Fe_3Ir(CO)_{12}]^{3-}$ cluster (*vide infra*). Three CO ligands were edge bridging on the Fe_2Ir equatorial plane. In addition, there were two terminal CO ligands on each atom (Fe or Ir) of the equatorial plane. The cluster was completed by three terminal CO ligands on the apical Fe and a PPh_3 ligand on Au. In addition, three short Au-C(O) contacts [2.775(2)-2.938(2) Å] were detected on the solid state structure. As previously discussed in the literature, it was debated if such short contacts were real interactions (even if very weak) or just the result of the steric orientation of the CO ligands [70]. The molecular structure of **7** closely resembled to that previously reported for $[Fe_2Ir_2(CO)_{12}(AuPPh_3)]^-$, where both Ir atoms were located on the equatorial plane [5].

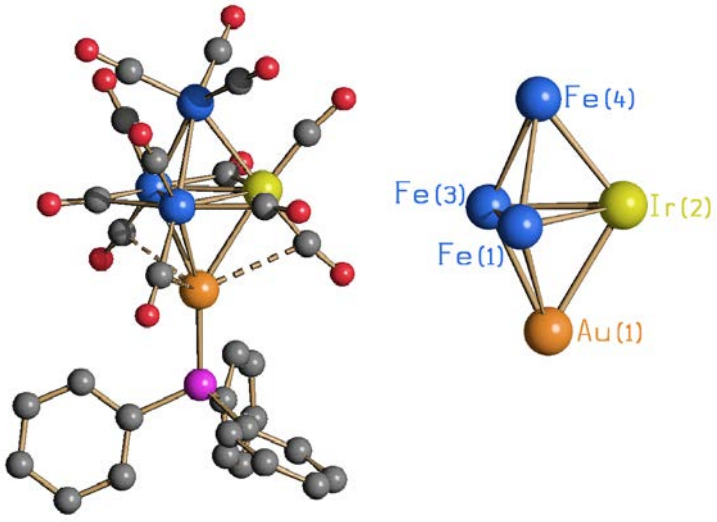

Fig. 4 (a) Molecular structure of $[Fe_3Ir(CO)_{12}(AuPPh_3)]^{2-}$ (**7**) and (b) its metal core with labeling (blue, Fe; yellow, Ir; grey, C; red, O; orange, Au; purple, P). H-atoms bonded to Ph-rings have been omitted for clarity. Au-C(O) contacts [2.775(2)-2.938(2) Å] are represented as fragmented lines.

The $[AuPPh_3]^+$ fragment was reported to be isolobal with H^+ [15-20]. Thus, it was of interest to compare the structure of **7** with the related hydride $[HFe_3Ir(CO)_{12}]^{2-}$ (**9**). Unfortunately, only a

partial structure of **9** was previously reported [6]. Thus, we attempted its synthesis and accurate crystal structure determination.

It must be remarked that **9** was originally obtained from $[HFe(CO)_4]^-$ and $[Ir(CO)_2Cl_2]^-$ in refluxing thf, but this synthesis was not selective [6]. Thus, we sought an alternative synthesis, and **9** was selectively prepared from the reaction of $[HFe_4(CO)_{12}]^{3-}$ (**8**) with $[Ir(COE)_2Cl]_2$ (COE = cyclo-octene). Conversely, as previously reported, **8** reacted with $[Ir(COD)Cl]_2$ resulting in the formation of **1** [1]. This was likely to be due to the different nature of COE (monodentate) and COD (bidentate) ligands. For sake of comparison, $[HFe_3Co(CO)_{12}]^{2-}$ (**10**) was obtained from **8** and $Co_2(CO)_8$.

The molecular structures of **9** and **10** were determined by SC-XRD on their $[NEt_4]^+$ salts (Figure 5 and Table 1). $[NEt_4]_2$[**10**] was isomorphous and isostructural with the previously reported $[NEt_4]_2[HFe_3Rh(CO)_{12}]$ ($[NEt_4]_2$[**11**]) (Space group *Pnma*) [71]. **10** and **11** displayed a tetrahedral structure with the hydride ligand μ_3-coordinated to the basal Fe_2M plane. A partial structure of $[NEt_4]_2$[**9**] was also previously reported, but the quality of the data was not good [6]. Nonetheless, these crystals were isomorphous to $[NEt_4]_2$[**10**] and $[NEt_4]_2$[**11**] (Space group *Pnma*), suggesting that they were also isostructural. Conversely, we obtained a polymorph of $[NEt_4]_2$[**9**] (Space group *C2/c*), in which the hydride ligand is μ-coordinated to the Ir_{basal}-Fe_{apical} edge. The stereochemistry of the CO ligands was identical in **9-11**, and consisted of three μ-CO ligands on the basal plane and nine terminal carbonyls (three on the apical atom, two on each of the three basal atoms).

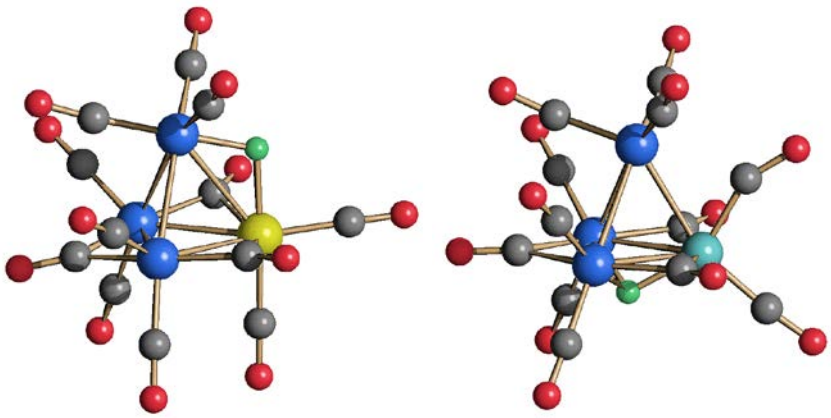

(a) (b)

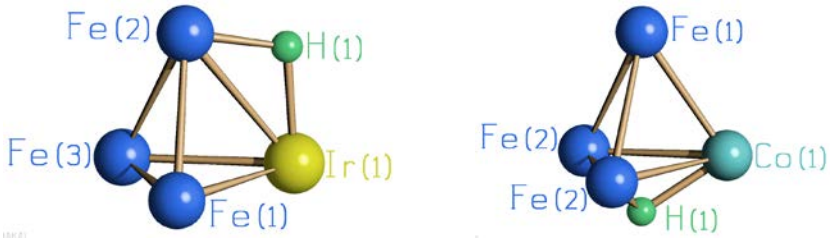

Fig. 5 Molecular structures of (a) $[HFe_3Ir(CO)_{12}]^{2-}$ (**9**) and (b) $[HFe_3Co(CO)_{12}]^{2-}$ (**10**) and their metal-hydride cages with labeling (blue, Fe; yellow, Ir; grey, C; red, O; green, H; cyan, Co). H-atoms bonded to Ph-rings have been omitted for clarity.

The isomerism in $[HFe_3M(CO)_{12}]^{2-}$ (M = Ir, **9**; M = Co, **10**; M = Rh, **11**) was computationally investigated, considering the hydride μ_3-coordinated to the basal Fe_2M plane (**face**) or μ-coordinated to M_{basal}-Fe_{apical} (**edge**). The optimized geometries are shown in Figure 6. In the case of the Ir derivative the μ-coordination of the hydride ligand to the Ir_{basal}-Fe_{apical} edge is more stable than the μ_3-bonding to basal face, in agreement with the structure reported in this work. On the other hand, Figure 6 highlights that the energy difference between **face** and **edge** isomers progressively reduces on replacing Ir with the lighter elements of its series, this supporting the possibility of polymorphism also for the Co and Rh derivatives **10** and **11**.

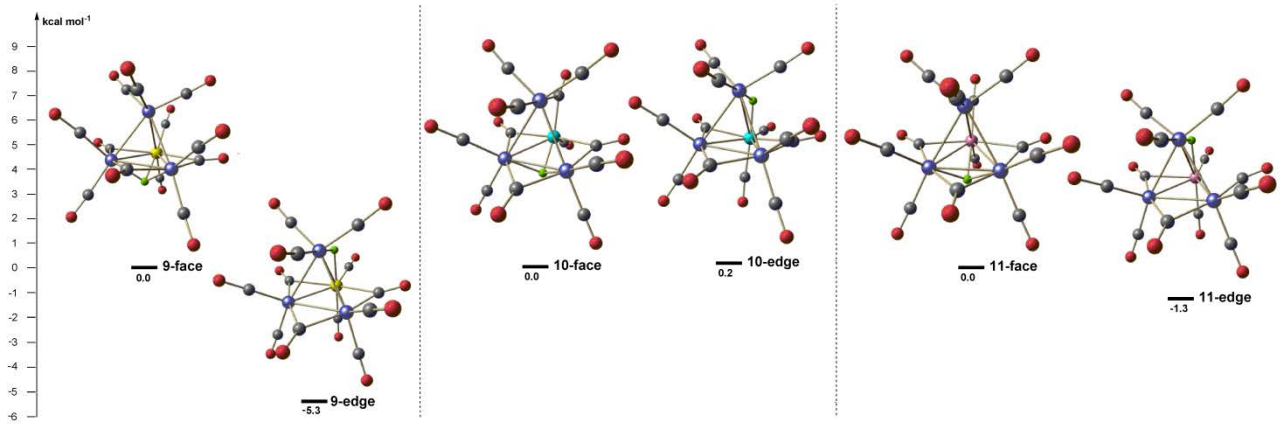

Fig. 6 DFT-optimized structures of the **face** and **edge** isomers of **9**, **10** and **11** and relative Gibbs energy values, referred to the **face** isomers (blue, Fe; cyan, Co; pink, Rh; yellow, Ir; grey, C; red, O; green, H).

Despite the H^+ ◯ $[AuPPh_3]^+$ isolobal analogy, the situation is markedly different for the Au-derivative **7**. DFT calculations confirmed that the μ_3-coordination to the basal Fe_2Ir plane (**7-face**) is more stable than the μ-bonding to the Ir_{basal}-Fe_{apical} edge (**7-edge**) by about 6.2 kcal mol^{-1}. The computed isomers are shown in Figure S6.

Conclusions

The new bimetallic Fe-Ir carbonyl clusters **2**, **3**, **5** and **6**, as well as the trimetallic Fe-Ir-Au species **7**, have been synthesised and fully characterized. Moreover, a straightforward synthesis and full structural characterization of the mono-hydride **9** has been reported. Clusters **2**, **5**, **6** and **9** contain a hydride ligand. It must be remarked that, despite the isolobal analogy, the $AuPPh_3$ fragment of **7** is located on a triangular Fe_2Ir face, whereas the hydride ligand of **9** is bridging on a Fe-Ir edge of the same Fe_3Ir tetrahedral cage. The hydride is conversely μ_3-coordinated to a Fe_2M (M = Co, Rh) face of the related mono-hydrides **10** and **11**. Hydride location on these clusters has been investigated by DFT methods, that revealed to be a very important tool in combination with SC-XRD analyses.

Experimental

General procedures.

All reactions and sample manipulations were carried out using standard Schlenk techniques under nitrogen and in dried solvents. All the reagents were commercial products (Aldrich) of the highest purity available and used as received, except $[NEt_4]_2$[**1**] [1], $[NEt_4]_3$[**8**] [72] $Au(PPh_3)Cl$ [73] and $[Ir(COE)_2Cl]_2$ [74] which have been prepared according to the literature. Analysis of Fe and Ir were performed by atomic absorption on a Pye-Unicam instrument. Analyses of C, H and N were obtained with a Thermo Quest Flash EA 1112NC instrument. IR spectra were recorded on a Perkin Elmer Spectrum One interferometer in CaF_2 cells. NMR measurements were performed on a Varian Mercury Plus 400 MHz instrument.Structure drawings have been performed with SCHAKAL99 [75].

Synthesis of $[NEt_4]_2[HFe_4Ir(CO)_{14}]$ ($[NEt_4]_2$[2])

$[NEt_4]_2$[**1**] (0.290 g, 0.258 mmol) was dissolved in CH_2Cl_2 (20 mL) and the resulting solution stirred at room temperature for 2 h under a gentle stream of CO (1 atm). The solvent was, then, removed *in vacuo* and the solid residue was washed with H_2O (20 mL) and toluene (40 mL) and the

product was finally extracted with CH_2Cl_2 (20 mL). Crystals of $[NEt_4]_2$[**2**] suitable for X-ray analyses were obtained by layering n-hexane (40 mL) on the CH_2Cl_2 solution (yield 0.206 g, 75 % based on Fe).

$C_{30}H_{41}Fe_4IrN_2O_{14}$ (1069.25): calcd. C 33.65, H 3.86, N 2.62, Ir 18.03, Fe 20.91; found: C 33.34, H 4.05, N 2.48, Ir 17.89, Fe 21.11. IR (nujol, 293 K) ν(CO): 2027(s), 1950(vs), 1895(sh), 1748(s), 1647(s) cm^{-1}. IR (CH_2Cl_2, 293 K) ν(CO): 2025(m), 1959(vs), 1902(sh), 1779(sh), 1751(s) cm^{-1}. IR (thf, 293 K) ν(CO): 2021(w), 1966(sh), 1955(vs), 1906(w), 1802(w), 1762(m) cm^{-1}. IR (acetone, 293 K) ν(CO): 2021(w), 1959(vs), 1906(w) cm^{-1}. IR (CH_3CN, 293 K) ν(CO): 2024(w), 1960(vs), 1907(w), 1790(w), 1758(s) cm^{-1}. IR (dmf, 293 K) ν(CO): 2021(w), 1967(w), 1958(vs), 1905(w), 1792(w), 1764(ms) cm^{-1}. ^{1}H NMR (CD_3COCD_3, 298 K) δ (ppm): -21.26 (s, 1H, hydride). ^{1}H NMR (CD_3COCD_3, 213 K) δ (ppm): -21.72 (s, 1H, hydride).

Synthesis of $[NEt_4][Fe_4Ir(CO)_{15}]$ ($[NEt_4]$[3])

$HBF_4{\cdot}Et_2O$ (35 □L, 0.253 mmol) was added to a solution of $[NEt_4]_2$[**2**] (0.135 g, 0.126 mmol) in CH_2Cl_2 (25 mL) and the resulting solution stirred at room temperature for 3 h. The solvent was, then, removed *in vacuo* and the solid residue was washed with H_2O (20 mL) and toluene (40 mL) and the product was finally extracted with CH_2Cl_2 (15 mL). Crystals of $[NEt_4]$[**3**] suitable for X-ray analyses were obtained by layering n-hexane (40 mL) on the CH_2Cl_2 solution (yield 0.050 g, 41% based on Fe).

$C_{23}H_{20}Fe_4IrNO_{15}$ (966.00): calcd. C 28.60, H 2.09, N 1.45, Ir 19.90, Fe 23.12; found: C 28.44, H 2.21, N 1.18, Ir 20.11, Fe 22.94. IR (nujol, 293 K) ν(CO): 2063(w), 2022(m), 1991(s), 1978(sh), 1932(w), 1800(m), 1746(w) cm^{-1}.

Synthesis of $[NEt_4][H_{1+x}Fe_{2+x}Ir_{2-x}(CO)_{10}(PPh_3)_2]{\cdot}CH_2Cl_2$ (x = 0, 1) ($[NEt_4]$[5-6]$\cdot CH_2Cl_2$)

PPh_3 (0.093 g, 0.356 mmol) was added as a solid to a solution of $[NEt_4]_2$[**1**] (0.200 g, 0.178 mmol) in CH_2Cl_2 (25 mL) and the resulting solution stirred at room temperature for 36 h. The solvent was, then, removed *in vacuo* and the solid residue was washed with H_2O (20 mL) and toluene (40 mL) and the product was finally extracted with CH_2Cl_2 (20 mL). Crystals of $[NEt_4]$[**5-6**]$\cdot CH_2Cl_2$ suitable for X-ray analyses were obtained by layering n-hexane (40 mL) on the CH_2Cl_2 solution (yield 0.100 g, 26 % based on Fe).

$C_{55}H_{53.63}Cl_2Fe_{2.63}Ir_{1.37}NO_{10}P_2$ (1431.15): calcd. C 46.11, H 3.78, N 0.98, Ir 18.47, Fe 10.28; found: C 46.34, H 3.94, N 1.12, Ir 18.25, Fe 10.09. IR (nujol, 293 K) ν(CO): 1980(m), 1936(w), 1904(s), 1856(sh), 1740(m), 1720(m) cm^{-1}. IR (CH_2Cl_2, 293 K) ν(CO): 1983(m), 1940(ms), 1914(s), 1878(sh), 1735(br) cm^{-1}. IR (acetone, 293 K) ν(CO): 1983(m), 1940(w), 1914(s), 1877(w) cm^{-1}. IR (CH_3CN, 293 K) ν(CO): 1983(m), 1941(w), 1877(w), 1771(sh), 1733(m), 1713(m) cm^{-1}. IR (dmf, 293 K) ν(CO): 1981(m), 1938(w), 1912(s), 1876(w), 1777(m) cm^{-1}. ^1H NMR (CD_3COCD_3, 298 K) δ (ppm): 7.49-7.27 (m, 30H, Ph), -16.54, -17.35 (s, 0.5 : 1, hydride). ^1H NMR (CD_3COCD_3, 213 K) δ (ppm): 7.30 (m, 30H, Ph), -16.72, -17.62 (s, 0.5 : 1, hydride). $^{31}P\{^1H\}$ NMR (CD_3COCD_3, 298 K) δ (ppm): 22.42 (s), 10.10 (s) (0.5 : 1). $^{31}P\{^1H\}$ NMR (CD_3COCD_3, 213 K) δ (ppm): 21.05 (s), 9.21 (s) (0.5 : 1).

Synthesis of $[NEt_4]_2[Fe_3Ir(CO)_{12}(AuPPh_3)]\cdot 0.5CH_2Cl_2$ ($[NEt_4]_2$[7]$\cdot 0.5CH_2Cl_2$)

$Au(PPh_3)Cl$ (0.465 g, 0.941 mmol) was added as a solid to a solution of $[NEt_4]_2$[**1**] (0.470 g, 0.418 mmol) in CH_3CN (20 mL) and the resulting solution stirred at room temperature for 48 h. The solvent was, then, removed *in vacuo* and the solid residue was washed with H_2O (20 mL) and toluene (40 mL) and the product was finally extracted with CH_2Cl_2 (20 mL) Crystals of $[NEt_4]_2$[**7**]$\cdot 0.5CH_2Cl_2$ suitable for X-ray analyses were obtained by layering n-hexane (40 mL) on the CH_2Cl_2 solution (yield 0.280 g, 34 % based on Fe, 45% based on Ir, 40% based on Au).

$C_{46.5}H_{56}AuClFe_3IrN_2O_{12}P$ (1458.07): calcd. C 38.30, H 3.87, N 1.92, Ir 13.18, Fe 11.49, Au 13.51; found: C 38.51, H 3.64, N 2.13, Ir 12.95, Fe 11.21, Au 13.77. IR (nujol, 293 K) ν(CO): 2037(m), 1966(vs), 1940(m), 1905(s), 1744(m) cm^{-1}. IR (CH_2Cl_2, 293 K) ν(CO): 2030(w), 1970(vs), 1955(sh), 1915(m), 1773(m) cm^{-1}. IR (thf, 293 K) ν(CO): 2039(w), 1968(vs), 1921(m), 1780(m) cm^{-1}. ^1H NMR (CD_2Cl_2, 298 K) δ (ppm): 6.73-7.24 (m, 15H, Ph), 2.50 (br, 8H, NCH_2CH_3), 0.91 (br, 12H, NCH_2CH_3). $^{13}C\{^1H\}$ NMR (CD_2Cl_2, 298 K) δ (ppm): 216.0 (CO), 133.9, 130.4, 128.7 (CH_{Ph}), 132.5 ($^1J_{C\text{-}P}$ = 47 Hz, C_{Ph}). $^{31}P\{^1H\}$ NMR (CD_2Cl_2, 298 K) δ (ppm): 55.6.

Synthesis of $[NEt_4]_2[HFe_3Ir(CO)_{12}]$ ($[NEt_4]_2$[9])

$[Ir(COE)_2Cl]_2$ (0.292 g, 0.326 mmol) was added to a solution of $[NEt_4]_3$[**8**] (0.310 g, 0.326 mmol) in CH_3CN (30 mL) and the resulting solution stirred at room temperature for 24 h. The solvent was, then, removed *in vacuo* and the solid residue was washed with H_2O (20 mL) and toluene (40 mL)

and the product was finally extracted with CH_2Cl_2 (15 mL). Crystals of $[NEt_4]_2$[**9**] suitable for X-ray analyses were obtained by layering n-hexane (40 mL) on the CH_2Cl_2 solution (yield 0.192 g, 46% based on Fe).

$C_{28}H_{41}Fe_3IrN_2O_{12}$ (957.38): calcd. 35.13, H 4.32, N 2.93, Ir 20.08, Fe 17.50; found: C 35.34, H 3.13, N 2.75, Ir 19.89, Fe 17.71. IR (nujol, 293 K) □(CO): 1985(vs) (acetone, 293 K) ν(CO): 2013(w), 1980(w), 1939(vs), 1896(w) cm^{-1}. IR (CH_3CN, 293 K) ν(CO): 2014(sh), 1983(w), 1942(vs), 1885(w), 1751(m) cm^{-1}. IR (dmf, 293 K) ν(CO): 2013(w), 1979(w), 1938(vs), 1878(m), 1760(m) cm^{-1}. ^1H NMR (CD_3COCD_3, 298 K) δ (ppm): -21.82 (s, 1H, hydride). ^1H NMR (CD_3COCD_3, 213 K) δ (ppm): -22.61 (s, 1H, hydride).

Synthesis of $[NEt_4]_2[HFe_3Co(CO)_{12}]$ ($[NEt_4]_2$[10])

$Co_2(CO)_8$ (0.420 g, 1.23 mmol) was added as a solid to a solution of $[NEt_4]_3$[**8**] (1.14 g, 1.20 mmol) in CH_3CN (30 mL) and the resulting solution stirred at room temperature for 3 h. The solvent was, then, removed *in vacuo* and the solid residue was washed with H_2O (20 mL) and toluene (40 mL) and the product was finally extracted with thf (20 mL). Crystals of $[NEt_4]_2$[**10**] suitable for X-ray analyses were obtained by layering toluene (40 mL) on the thf solution (yield 0.645 g, 49% based on Fe).

$C_{28}H_{41}CoFe_3N_2O_{12}$ (824.11): calcd. C 40.81, H 5.01, N 3.40, Co7.15, Fe 20.33; found: C 41.07, H 5.24, N 3.11, Co 6.91, Fe 20.49. IR (CH_3CN, 293 K) ν(CO): 2011(w), 1944(vs), 1891(w), 1784(m), 1758(m) cm^{-1}.

X-ray Crystallographic Study.

Crystal data and collection details for $[NEt_4]_2$[**2**], $[NEt_4]$[**3**], $[NEt_4][H_{1+x}Fe_{2+x}Ir_{2-x}(CO)_{10}(PPh_3)_2]\cdot CH_2Cl_2$ (x = 0, 1; a mixture of **5** and **6**), $[NEt_4]_2$[**7**]·0.5CH_2Cl_2, $[NEt_4]_2$[**9**] and $[NEt_4]_2$[**10**] are reported in Table S1 in the Supporting Information. The diffraction experiments were carried out on a Bruker APEX II diffractometer equipped with a CCD detector using Mo–Kα radiation. Data were corrected for Lorentz polarization and absorption effects (empirical absorption correction SADABS) [76]. Structures were solved by direct methods and refined by full-matrix least-squares based on all data using F^2 [77]. Hydrogen atoms were fixed at calculated positions and refined by a riding model, except hydride atoms which have been located in the Fourier map and

refined isotropically. All non-hydrogen atoms were refined with anisotropic displacement parameters, unless otherwise stated.

$[NEt_4]_2$[2]: The asymmetric unit of the unit cell contains four cluster anions and eight $[NEt_4]^+$ cations all located on general positions. The four cluster anions display very similar geometries and bonding parameters. Because of the presence of several independent molecules containing at the same time heavy and light atoms, several restraints have been employed during the refinement. In addition, the crystal is racemically twinned with a refined Flack parameter of 0.384(6) [78] and it was, therefore, refined using the TWIN refinement routine of SHELXTL. The hydride atom of each independent cluster anion was located in the Fourier map and refined isotropically, using the 1.2 fold U_{iso} value of the parent Fe atoms; the Fe-H distances were restrained within each anion to be similar (SADI line in SHELXL, s.u. 0.02). All the C and O-atoms have been restrained to isotropic behaviour (ISOR line in SHELXL, s.u. 0.01). One $[NEt_4]^+$ cation is disordered over two positions; disordered atomic positions were split and refined using one occupancy parameter per disordered group and restrained to have similar geometries (SAME line in SHELXTL, s.u. 0.02). The $[NEt_4]^+$ cations have been restrained to have similar *U* parameters (SIMU line in SHELXL, s.u. 0.01). Restraints to bond distances of the $[NEt_4]^+$ cations were applied as follow (s.u. 0.01): 1.47 C for C–N and 1.53 Å for C–C.

$[NEt_4]$[3]: The asymmetric unit of the unit cell contains half of a cluster anion (located on 2) and one $[NEt_4]^+$ cation (located on a general position). The crystal is racemically twinned with a refined Flack parameter of 0.58(3) [78] and it was, therefore, refined using the TWIN refinement routine of SHELXTL. The position occupied by M(1) is disordered Fe/Ir, with occupancy factors 0.5 : 0.5. Ir(1) and Fe(1) were constrained to have the same anisotropic displacement parameters [EADP line in SHELXL] and the same coordinated [EXYZ line in SHELXL]. The $[NEt_4]^+$ cation is disordered over four positions two by two related by an inversion centre; the independent disordered atomic positions were split and refined using one occupancy parameter per disordered group and restrained to have similar geometries (SAME line in SHELXTL, s.u. 0.02). The $[NEt_4]^+$ cations have been restrained to have similar *U* parameters (SIMU line in SHELXL, s.u. 0.01). Restraints to bond distances of the $[NEt_4]^+$ cations were applied as follow (s.u. 0.01): 1.47 C for C–N and 1.53 Å for C–C.

$[NEt_4][H_{1+x}Fe_{2+x}Ir_{2-x}(CO)_{10}(PPh_3)_2]\cdot CH_2Cl_2$ (x = 0, 1; a mixture of 5 and 6): The asymmetric unit of the unit cell contains one cluster anion (located on a general position), two halves of two

$[NEt_4]^+$ cations (located on 2), and one CH_2Cl_2 molecule (located on a general position). One of the four vertices of the M_4 tetrahedron of the cluster anion appears to be partially occupied by Ir(2) [refined occupancy factor 0.37(2)] and Fe(3) [refined occupancy factor 0.63(2)]. Ir(2) and Fe(3) were constrained to have the same anisotropic displacement parameters [EADP line in SHELXL]. The H(1) and H(3) hydride atoms were located in the Fourier map and refined isotropically, using the 1.2 fold U_{iso} value of the parent Ir and Fe atoms. The Fe-H distances were restrained to 1.69 Å, whereas Ir-H distances were restrained to 1.93 Å. In view of the diamagnetic nature of the clusters and their NMR spectra, H(1) has been included with occupancy factor 1, whereas H(3) has been included only together with Fe(3). This results in a co-crystallized mixture of two diamagnetic clusters, *i.e.*, **5** (*ca.* 37%) and **6** (*ca.* 63%). The Ph rings of the PPh_3 ligands were constrained to fit regular hexagons [AFIX 66 line in SHELXL]. One of the two halves of the two $[NEt_4]^+$ cations is disordered over four positions two by two related by a 2-fold axis; the independent disordered atomic positions were split and refined using one occupancy parameter per disordered group and restrained to have similar geometries (SAME line in SHELXTL, s.u. 0.02) and isotropic behaviour (ISOR line in SHELXTL, s.u. 0.01). Similar *U* restraints have been applied to the C and N atoms of the $[NEt_4]^+$ cation (SIMU line in SHELXL, s.u. 0.01). Restraints to bond distances were applied as follow (s.u. 0.01): 1.47 C for C–N and 1.53 Å for C–C in $[NEt_4]^+$; 1.75 Å for C–Cl in CH_2Cl_2.

$[NEt_4]_2$[7]·0.5CH_2Cl_2: The asymmetric unit of the unit cell contains one cluster anion and two $[NEt_4]^+$ cations located on general positions, and half of a CH_2Cl_2 molecule disordered over two equally populated symmetry related (by an inversion centre) positions. The three metal positions in the equatorial plane of the cluster are disordered Fe/Ir. The occupancy factor of each position has been refined, restraining the overall content of Ir to be one [SUMP 2 0.1 1 2 1 3 1 4 line in SHELXL]. One $[NEt_4]^+$ cation is disordered over two positions; disordered atomic positions were split and refined using one occupancy parameter per disordered group and restrained to have similar geometries (SAME line in SHELXTL, s.u. 0.02). The $[NEt_4]^+$ cations have been restrained to have similar *U* parameters (SIMU line in SHELXL, s.u. 0.01). Restraints to bond distances of the $[NEt_4]^+$ cations were applied as follow (s.u. 0.01): 1.47 C for C–N and 1.53 Å for C–C.

$[NEt_4]_2$[9]: The asymmetric unit of the unit cell contains one cluster anion and two $[NEt_4]^+$ cations all located on general positions. The hydride atom was located in the Fourier map and refined isotropically, using the 1.2 fold U_{iso} value of the parent atom. The Fe-H distance was restrained to

1.67 Å, whereas Ir-H distance was restrained to 1.93 Å (s.u. 0.02). Restraints to bond distances of the $[NEt_4]^+$ cations were applied as follow (s.u. 0.02): 1.47 C for C–N and 1.53 Å for C–C.

$[NEt_4]_2$[10]: The asymmetric unit of the unit cell contains one half of a cluster anion (located on m) and two halves of two $[NEt_4]^+$ cations (one located on m and one on an inversion centre). The hydride atom was located in the Fourier map and refined isotropically, using the 1.2 fold U_{iso} value of the parent atom. The $[NEt_4]^+$ cations are disordered over four positions two by two related by an inversion centre or a mirror plane; the independent disordered atomic positions were split and refined using one occupancy parameter per disordered group. Restraints to bond distances of the $[NEt_4]^+$ cations were applied as follow (s.u. 0.02): 1.47 C for C–N and 1.53 Å for C–C.

CCDC 2002502-2002507 contain the supplementary crystallographic data for this paper.

Computational details

Geometry optimizations were carried out using the PBEh-3c method, which is a reparametrized version of PBE0 (with 42% HF exchange) that uses a split-valence double-zeta polarized basis set (def2-mSVP) for light atoms. 28 electrons of Rh and 60 electrons of Ir are included in relativistic ECPs. The method adds three corrections that consider dispersion, basis set superposition and other basis set incompleteness effects [79]. The “restricted” approach was used in all the cases. Calculations were performed with the ORCA 4.0.1.2 software [80-81]. The output, converted in .molden format, was used Hirshfeld analyses, performed with the software Multiwfn, version 3.5 [82]. Cartesian coordinates of the DFT-optimized structures are collected in a separated .xyz file.

References

1. M. Bortoluzzi, I. Ciabatti, C. Femoni, M. Hayatifar, M. C. Iapalucci, and S. Zacchini (2015). *Organometallics* 34, 189.
2. R. Della Pergola, L. Garlaschelli, F. Demartin, M. Manassero, N. Masciocchi, M. Sansoni, and A. Fumagalli (1989). *J. Chem. Soc. Dalton Trans.* 1109.
3. W. L. Gladfelter, and G. L Geoffrey (1980). *Adv. Organomet. Chem.* 18, 207.
4. R. Della Pergola, L. Garlaschelli, F. Demartin, M. Manassero, N. Masciocchi, and G. Longoni (1988). *J. Chem. Soc. Dalton Trans.* 201.
5. R. Della Pergola, L. Garlaschelli, F. Demartin, M. Manassero, N. Masciocchi, and M. Sansoni (1990). *J. Chem. Soc. Dalton Trans.* 127.

6. A. Ceriotti, R. Della Pergola, L. Garlaschelli, F. Laschi, M. Manassero, N. Masciocchi, M. Sansoni, and P. Zanello (1991). *Inorg. Chem.* 30, 3349.
7. R. Della Pergola, A. Ceriotti, L. Garlascelli, F. Demartin, M. Manassero, N. Masciocchi, and M. Sansoni (1993). *Inorg. Chem.* 32, 3277.
8. E. Guggolz, M. L. Ziegler, W. Kalcher, J. Plank, D. Riedel, and W. A. Hermann (1981). *Z. Naturforsch. B* 36, 1053.
9. J. Chen, L. M. Daniels, and R. J. Angelici (1991). *J. Am. Chem. Soc.* 113, 2544.
10. R. Della Pergola, L. Garlaschelli, M. Manassero, C. Manassero, A. Sironi, D. Strumolo, S. Fedi, E. Grigiotti, and P. Zanello (2009). *Inorg. Chim. Acta* 362, 331.
11. M. I. Bruce, G. A. Koutsantonis, and E. R. T. Tienkink (1991). *J. Organomet. Chem.* 408, 77.
12. M. I. Bruce, G. A. Koutsantonis, and E. R. T. Tienkink (1991). *J. Organomet. Chem.* 407, 391.
13. A. Franken, T. D. McGrath, and F. G. A. Stone (2008). *Organometallics* 27, 148.
14. M. I. Bruce, P. E. Corbin, P. A. Humphrey, G. A. Koutsantonis, M. J. Liddel, and E. R. T. Tiekink (1990). *Chem. Commun.* 674.
15. J. W. Lauher, and K. Wald (1981). *J. Am. Chem. Soc.*103, 7648.
16. P. Braunstein, J. Rosé, Y. Dusausoy, and J.–P. Mangeot (1982). *C. R. Chim.*294, 967.
17. X. Li, B. Kiran, and L.-S. Wang (2005). *J. Phys. Chem. A*109, 4366.
18. R. Hoffmann (1982). *Angew. Chem. Int. Ed.*21, 711.
19. D. M. P. Mingos (1984). *Gold Bull.*17, 5.
20. P. Braunstein, and J. Rosé (1985). *Gold Bull.*18, 17.
21. I. Ciabatti, C. Femoni, M. Hayatifar, M. C. Iapalucci, A. Ienco, G. Longoni, G. Manca, and S. Zacchini (2014). *Inorg. Chem.* 53, 9761.
22. H. Schmidbaur, and A. Schier (2012). *Chem. Soc. Rev.* 41, 370.
23. P. Pyykkö (1997). *Chem. Rev.***97**, 597.
24. H. Schmidbaur, and A. Schier (2008). *Chem. Soc. Rev.***37, 1932.**
25. P. Pyykkö (2008). *Chem. Soc. Rev*. **37**, 1967.
26. S. Sculfort, and P. Braunstein (2011). *Chem. Soc. Rev.***40**, 2741.
27. M. Bortoluzzi, I. Ciabatti, C. Femoni, M. Hayatifar, M. C. Iapalucci, G. Longoni, and S. Zacchini (2014). *Angew. Chem. Int. Ed.* **53, 7233.**

28. M. Bortoluzzi, I. Ciabatti, C. Cesari, C. Femoni, M. C. Iapalucci, and S. Zacchini (2017). *Eur. J. Inorg. Chem.* 3135.
29. M. Bortoluzzi, C. Cesari, I. Ciabatti, C. Femoni, M. Haytifar, M. C. Iapalucci, R. Mazzoni, and S. Zacchini (2017). *J. Clust. Sci.***28**, 703.
30. I. Ciabatti, C. Femoni, M. C. Iapalucci, S. Ruggieri, and S. Zacchini (2018). *Coord. Chem. Rev.* **355**, 27.
31. B. Berti, M. Bortoluzzi, C. Cesari, C. Femoni, M. C. Iapalucci, R. Mazzoni, F. Vacca, and S. Zacchini (2019). *Inorg. Chem.***58**, 2911.
32. B. Berti, M. Bortoluzzi, C. Cesari, C. Femoni, M. C. Iapalucci, R. Mazzoni, F. Vacca, S. Zacchini (2019) *Eur. J. Inorg. Chem.* 3084.
33. B. Berti, M. Bortoluzzi, C. Cesari, C. Femoni, M. C. Iapalucci, R. Mazzoni, F. Vacca, S. Zacchini (2020) *Inorg. Chem.* **59**, 2228.
34. M. Bortoluzzi, A. Ceriotti, C. Cesari, I. Ciabatti, R. Della Pergola, C. Femoni, M. C. Iapalucci, A. Storione, S. Zacchini (2016) *Eur. J. Inorg. Chem.* 3939.
35. C. Cesari, I. Ciabatti, C. Femoni, M. C. Iapalucci, F. Mancini, S. Zacchini (2017) *Inorg. Chem.* **2017**, 1655.
36. B. Berti, C. Cesari, F. Conte, I. Ciabatti, C, Femoni, M. C. Iapalucci, F. Vacca, S. Zacchini (2018) *Inorg. Chem.***2018**, 7578.
37. M. Bortoluzzi, C. Cesari, I. Ciabatti, C. Femoni, M. C. Iapalucci, S. Zacchini (2017) *Inorg. Chem.* **56**, 6532.
38. R. D. Adams, and B. Captain (2004). *J. Organomet. Chem.* **689**, 4521.
39. R. D. Adams, and F. A. Cotton (Eds.). *Catalysis by Di- and Polynuclear Metal Cluster Complexes* (Wiley-VCH, New York, 1998).
40. J. M. Thomas, B. F. G. Johnson, R. Raja, G. Sankar, and P. A. Midgley (2003). *Acc. Chem. Res.* **36**, 20.
41. B. F. G. Johnson (2003). *Top. Catal.* **24**, 147.
42. S. Hermans, R. Raja, J. M. Thomas, B. F. G. Johnson, G. Sankar, and D. Gleeson (2001). *Angew. Chem. Int. Ed.* **40**, 1211.
43. R. D. Adams, and E. Trufan (2010). *Phil. Trans. R. Soc. A* **368**, 1473.
44. S. Zacchini (2011). *Eur. J. Inorg. Chem.* 4125.

45. D. S. Shephard, T. Maschmeyer, G. Sankar, J. M. Thomas, D. Ozkaya, B. F. G. Johnson, R. Raja, R. D. Oldroyd, and R. G. Bell (1998). *Chem. Eur. J.* **4**, 1214.
46. R. D. Adams, D. A. Blom, B. Captain, R. Raja, J. M. Thomas, and E. Trufan (2008). *Langmuir* **24**, 9223.
47. R. Bonelli, S. Albonetti, V. Morandi, L. Ortolani, P. M. Riccobene, S. Scirè, and S. Zacchini (2011). *Appl. Catal A* **395**, 10.
48. R. Bonelli, C. Lucarelli, T. Pasini, L. F. Liotta, S. Zacchini, and S. Albonetti (2011). *Appl. Catal A* **400**, 54.
49. D. Bonincontro, A. Lolli, A. Storione, A. Gasparotto, B. Berti, S. Zacchini, N. Dimitratos, and S. Albonetti (2019). *Appl. Catal A* **588**, 117279.
50. F. Schweyer-Tihay, C. Estournès, P. Braunstein, J. Guille, J. L. Paillaud, M. Richard-Plouet, and J. Rosé (2006).*Phys. Chem. Chem. Phys*. **8**, 4018.
51. S. Marengo, R. Psaro, C. Dossi, S. Calmotti, and R. Della Pergola (1996). *Stud. Surf, Sci. Catal.* 101, 1411.
52. R. Ugi, C. Dossi, and R. Psaro (1996). *J. Mol. Catal. A* 107, 13.
53. T. Kimura, A. Fukuoka, A. Fumagalli, and M. Ichikawa (1989). *Catal. Lett.* 2, 227.
54. T. Venäläinen, E. Iiskola, J. Pursianen, T. A. Pakkanen, and T. T. Pakkanen (1986). *J. Mol. Catal.* 34, 293.
55. A. Fukuoka, T. Kimura, N. Kusogi, H. Kuroda, Y. Minai, Y. Sakai, T. Tominaga, and M. Ichikawa (1990). *J. Catal.* 126, 434.
56. A. G. Orpen, L. Brammer, F. H. Allen, O. Kennard, D. G. Watson, and R. Taylor (1989). *J. Chem. Soc., Dalton Trans.* S1.
57. C. Femoni, M. C. Iapalucci, G. Longoni, and S. Zacchini (2011). *Dalton Trans.* 40, 8685.
58. S. M. Owen (1988). *Polyhedron* 7, 253.
59. D. M. P. Mingos, and R. L. Johnson (1987). *Struct. Bonding (Berlin)* 68, 29.
60. A. Ceriotti, M. Daghetta, S. El Afefey, A. Ienco, G. Longoni, G. Manca, C. Mealli, S. Zacchini, and S. Zarra (2011). *Inorg. Chem.* 50, 12553.
61. K. C. C. Kharas, and L. F. Dahl (1988). *Adv. Chem. Phys.* 70, 1.
62. R. D. Adams, and M. Chen (2011). *Inorg. Chem.* 30, 5867.
63. R. Della Pergola, L. Garlaschelli, M. Manassero, M. Sansoni, and S. Strumolo (2001). *J. Clust. Sci.* 12, 23.

64. R. D. Adams, and M. Chen (2012). *Organometallics* 31, 445.
65. D. F. Shriver, H. D. Kaesz, and R. D. Adams (Eds.) (1990). *The Chemistry of Metal Cluster Complexes*. VCH, New York.
66. G. Longoni, P. Chini, L. D. Lower, and L. F Dahl (1975). *J. Am. Chem. Soc.* 97, 5034.
67. A. Fumagalli, T. F. Koetzle, F. Takusagawa, P. Chini, S. Martinenfo, and B. T. Heaton (1980). *J. Am. Chem. Soc.* 102, 1740.
68. 66A. Fumagalli, T. F. Koetzle, and F. Takusagawa (1981). *J. Organomet. Chem.* 213, 365.
69. A. Fumagalli, and G. Ciani (1984). *J. Organomet. Chem.* 272, 91.
70. P. Braunstein, J. Rosé, A. Dedieu, Y. Dusausoy, J.-P. Mangeot, A. Tiripicchio, and M. Tiripicchio-Camellini (1986). *J. Chem. Soc., Dalton Trans.* 225.
71. R. Della Pergola, L. Garlaschelli, F. Demartin, M. Manassero, N. Masciocchi, and G. Longoni (1988). *J. Organomet. Chem.* 352, C59.
72. C. Femoni, M. C. Iapalucci, G. Longoni, S. Zacchini, and S. Zarra (2009). *Inorg. Chem.* 48, 1599.
73. C. Kowala, and J. M. Swan (1966). *Aust. J. Chem.* 19, 547.
74. J. L. Herde, J. C. Lambert, and C. V. Senoff (1974). *Inorg. Synth.* 15, 18.
75. E. Keller *SCHAKAL99* (University of Freiburg, Germany, 1999)
76. G. M. Sheldrick*SADABS-2008/1 – Bruker AXS Area Detector Scaling ans Absorption Correction* (Bruker AXS, Madison, Wisconsin, USA, 2008).
77. G. M. Sheldrick (2015). *Acta Crystallogr., Sect. C* 71, 3.
78. H. D. Flack (1983). *Acta Crystallogr., Sect A* 39, 876.
79. S. Grimme, J. G. Brandenburg, C. Bannwarth and A. Hansen (2015). *J. Chem. Phys.* 143, 054107.
80. F. Neese (2012). *WIREs Comput. Mol. Sci.* 2, 73.
81. F. Neese (2018). *WIREs Comput. Mol. Sci.* 8, e1327.
82. T. Lu and F. Chen (2012). *J. Comput. Chem.* 33, 580.